Direct electron transfer of fructose dehydrogenase immobilized on thiol-gold electrodes

Yan, Xiaomei; Ma, Su; Tang, Jing; Tanner, David; Ulstrup, Jens; Xiao, Xinxin; Zhang, Jingdong

Published in:
Electrochimica Acta

Link to article, DOI:
10.1016/j.electacta.2021.138946

Publication date:
2021

Document Version
Publisher's PDF, also known as Version of record

Electrochimica Acta 392 (2021) 138946

Contents lists available at ScienceDirect

Electrochimica Acta

journal homepage: www.elsevier.com/locate/electacta

Direct electron transfer of fructose dehydrogenase immobilized on thiol-gold electrodes

Xiaomei Yan[a], Su Ma[b], Jing Tang[a], David Tanner[a], Jens Ulstrup[a], Xinxin Xiao[a,*], Jingdong Zhang[a]

[a] Department of Chemistry, Technical University of Denmark, Kongens Lyngby 2800, Denmark
[b] Biocatalysis and Biosensing Laboratory, Department of Food Science and Technology, BOKU-University of Natural Resources and Life Sciences, Muthgasse 18, Vienna 1190, Austria

ARTICLE INFO

Article history:
Received 27 April 2021
Revised 29 June 2021
Accepted 18 July 2021
Available online 27 July 2021

Keywords:
Direct electron transfer
Self-assembled monolayers
Fructose dehydrogenase
Au(111)
Nanoporous gold

ABSTRACT

Direct electrochemical electron transfer (DET) of oxidoreductases has attracted increasing attention in pure and applied bioelectrochemistry (e.g. biosensors and biofuel cells) over the last decades. We report here a systematic study of DET-type bioelectrocatalysis of the membrane-bound redox enzyme fructose dehydrogenase (FDH, *Gluconobacter sp.*), on variable-length and variably terminated thiol self-assembled monolayers (SAMs) both on Au(111) and nanoporous gold (NPG) electrodes. FDH on Au(111) modified by short-chain moderately hydrophilic 2-mercaptoethanol (BME) SAMs exhibits the highest DET activities and largest DET-capable fraction. Fitting of theoretical polarization curves to the data and homology modeling/docking of FDH offer further mechanistic insight. The dependence of the DET efficiency of FDH on the length and differently terminated carbon chain is systematically presented. The decreased DET rate with increasing chain length is associated with increasingly unfavourable long-range electron tunnelling, and not with lowered enzyme loading. The porous structure of NPG is favorable for FDH bioelectrocatalysis by improving both efficient enzyme orientation and operational stability. Overall, our study maps systematically the controlled local environmental structural flexibility of the Au/SAM/enzyme/solution interface, a paradigm for thiol modified surfaces in biosensors and bioelectronics.

1. Introduction

Electron transfer (ET) between an electrode surface and the redox/catalytic center(s) of oxidoreductases is one of the most important processes in enzyme bioelectronics including biosensors and enzymatic biofuel cells (EBFCs) [1,2]. Two types of ET processes have been studied over the past decades, mediated ET (MET) and direct ET (DET) [3,4]. In MET, redox mediators with suitable redox potentials shuttle electrons between the electrode surface and the enzyme redox centers especially if the latter are deeply buried inside the protein [5]. Appropriate enzyme orientation and high enzyme loading on the electrodes are, however, critical for the ET rate and catalytic current density in DET-type reactions [6]. A wide range of enzymes capable of DET have been reported [7–11]. The enzymes typically harbour cofactors or built-in redox centers close to the protein surfaces, allowing efficient electron tunneling, if properly positioned on the electrode surface.

FDH (EC 1.1.99.11) from *Gluconbacter japonicas* (molecular mass: ~140 kDa), central in carbohydrate metabolism, consists of three subunits: subunit I (67 kDa), subunit II (51 kDa) and subunit III (20 kDa) [12]. Subunit I contains a flavin adenine dinucleotide (FAD) cofactor as the catalytic center of two-electron D-fructose oxidation into keto-D fructose. Subunit II holds three heme *c* moieties, serving as ET relays between external electron acceptors and FAD, Scheme 1. Subunit III has no redox active centers and possibly contributes to the structural integrity of the enzyme. FDH holds promise for applications in bioelectrochemistry because of its oxygen insensitivity, high catalytic performance, and long-time stability under mild conditions [13,14]. It is widely accepted that the DET pathway on the electrode involves only two hemes, heme 3*c* and 2*c*, with the relatively low formal potentials ($E^{o'}$) (ca. -0.01 and 0.06 V vs. Ag/AgCl at pH 5.5) [15], while the higher $E^{o'}$ of 0.15 V of the third heme, heme 1*c*, disfavors this heme group in the ET sequence [12,16,17].

To achieve efficient DET of FDH, it is important to know the character of the enzyme surface properties and engineer the electrode surfaces for favourable enzyme orientation and distances be-

* Corresponding author.
E-mail address: xixiao@kemi.dtu.dk (X. Xiao).

https://doi.org/10.1016/j.electacta.2021.138946

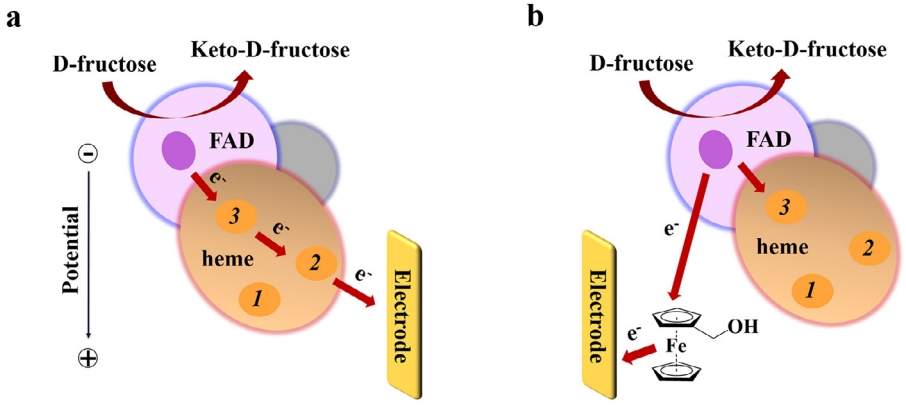

Scheme 1. Schematic illustration of possible ET pathway from FAD in D-fructose to the electrode undergoing (a) DET and (b) MET. Eo' (vs. Ag/AgCl) follows the sequence: heme 3c (-0.01 V) < heme 2c (0.06 V) < heme 1c (0.15 V) < FcMeOH (0.23 V).

tween the heme relays and the electrode surfaces. However, the crystal structure of FDH is still unknown, which poses a challenge to full understanding of the enzyme function at the molecular level. FDH is a membrane-bound enzyme with subunit II anchored to the membrane [6]. The amino acid sequence suggests the presence of a C-terminal hydrophobic region (CHR) of subunit II [18]. Several groups have suggested that a hydrophobic electrode surface functionalized with anthracene or naphthoquinone is favourable for DET of FDH [17,19], but favourable conductive supports with hydrophilic radicals have been reported in other studies [20,21]. The isoelectric point (IEP) of FDH is estimated to be 6.59, leading to an overall positively charged surface in slightly acidic solutions (pH 5.5 typical for FDH immobilization and testing) [22]. This is most likely the reason why several studies used negatively charged surfaces to address the DET of FDH [11,22,23], but comparative studies using differently functionalized electrode surfaces are clearly desirable.

Self-assembled molecular monolayers (SAMs) of thiol based molecules on gold electrodes bound *via* Au-S bond formation, are versatile by providing a variety of terminal groups, such as carboxyl, hydroxyl and amino groups [24,25]. Differently charged thiols (4-mercaptobenzoic acid (4-MBA), 4-mercaptophenol (4-MPh), and 4-aminothiophenol (4-APh)) have been immobilized on porous gold electrodes in studies of FDH electrocatalysis, with an uncharged hydrophilic electrode surface with a hydroxyl group (4 MPh) found to display the highest DET current density [22]. A similar study by Murata and associates reported that FDH anchored on gold nanoparticles (AuNPs) functionalized with 2-mercaptoethanol (BME) SAMs exhibits the highest current density in DET-type bioelectrocatalysis, exceeding that of both 3-mercaptopropionic acid (MPA, negative) and 2-aminoethanethiol (AET, positive) [25]. Kawai and associates also found that the hydrophilic BME-modified electrode is more efficient in DET than 2-mercaptoethane (ME)-modified hydrophobic electrodes [26]. Among these reports, a moderately hydrophilic surface with terminal hydroxyl groups is thus found to be optimal. However, enzyme loading and the fraction of the total amount of immobilized FDH enzyme capable of DET are not well documented. Xia and associatesinvestigated the relative activity of FDH on Ketjen black electrodes modified with various methoxy aromatic amines, showing that similar enzyme loadings on different electrodes were obtained [27]. It was proposed that the highest DET activity obtained with a methoxy substituent could be attributed to the most favourable enzyme surface orientation rather than most favourable enzyme loading [27]. However, a systematic understanding of factors underlying the observed or proposed superior DET behavior is not available.

Introduction of nanomaterials into DET-type bioelectrochemistry represents other major progress over the last decades. The utilization of nanomaterials, especially porous metallic or semimetallic nanomaterials, improves both enzyme loading and stability, facilitates productive enzyme orientation, and thus enhances the DET performance [10,28]. Funabashi and associates investigated MgO-templated porous carbons (MgOCs) with pore diameters of 10, 20, 40, 100 nm for DET of FDH [29]. The size of FDH is estimated to show efficient catalytic performance with the pore diameters (20 and 40 nm), as more enzyme can permeate the porous structure with pore sizes significantly wider than the enzyme size. FDH embedded in MgOCs with the smaller pore width of 20 nm exhibits high stability, as narrow pores appear to reduce aggregation and collision of enzyme molecules. Nanoporous gold (NPG) materials with average pore diameters ranging from 9–62 nm for FDH immobilization under different de-alloying conditions have been synthesized [23]. NPG with a moderate pore diameter of 42 nm showed the best DET-type current density, probably due to the highest enzyme loading. As long as the pore diameter is larger than the enzyme, the smaller pore diameter leads to larger surface area and higher enzyme loading. However, when the pore diameter is smaller than the enzyme, NPG cannot load more enzyme molecules. NPG with a medium pore size therefore typically offers the highest enzyme loading [28].

In this work, we have conducted systematic investigations both of the effects of variable-length and variably terminated thiol SAMs, and of NPG support compared to single-crystal Au(111) structure in DET-type bioelectrocatalysis of FDH. Au(111)-electrodes are convenient for mapping the kinetic mechanisms of the interfacial DET processes in bioelectrocatalysis due to their low background currents, well-defined atomically planar surfaces, and relatively easy modification with thiol SAMs. Homology modeling/docking studies of FDH were conducted to rationalise in greater detail, and at the molecular level, the interaction between the FDH target enzyme molecule and the differently terminated SAMs. Fitting of theoretical electrocatalytic profiles to the data was undertaken for further mechanistic mapping. The catalytic properties were found to depend strongly both on the alkyl chain length, with a significant decrease with increasing SAM carbon chain length, and on the nature of the terminal group. Finally, the porous NPG structure gives notably larger amounts of active enzyme capable both of DET and of MET-type catalytic current densities, as well as significantly higher operational stability compared with Au(111)-electrodes. Such a comprehensive study, involving most of the interfacial structure-functional properties of a complex bioelectrochemical interface, has not been reported before.

2. Experimental section

2.1. Chemicals and materials

FDH from *Gluconobacter sp.* (EC 1.1.99.11, activity 145 U mg^{-1}) was from Sorachim Chemicals, Switzerland. Cysteamine hydrochloride ($HS(CH_2)_2NH_2$•HCl, MEA, ≥ 98%), 2-mercaptoethanol ($HS(CH_2)_2OH$, BME, ≥ 99.0%), 3-mercaptopropanoic acid ($HS(CH_2)_2COOH$, MPA, ≥ 99.0%), propanethiol ($HS(CH_2)_2CH_3$, PPT, 99%), 3-mercapto-1-propanol ($HS(CH_2)_3OH$, 95%), 6-mercapto-1-hexanol ($HS(CH_2)_6OH$, 97%), 9-mercapto-1-nonanol ($HS(CH_2)_9OH$, 96%), 11-mercapto-1-undecanol ($HS(CH_2)_{11}OH$, 97%), hydrochloride acid (HCl, 37%), sulfuric acid (H_2SO_4, 95–97%), citric acid ($HOC(COOH)(CH_2COOH)_2$, ≥ 99.5%), sodium monohydrogen phosphate dodecahydrate (Na_2HPO_4•$12H_2O$, ≥ 99.0%), fructose (≥ 99.0%), hydroxymethylferrocene (FcMeOH, 97%), Triton X-100 (~10% in H_2O), potassium hexacyanoferrate(III) ($K_3[Fe(CN)_6]$, 99%), iron(III) sulfate ($Fe_2(SO_4)_3$, 97%), sodium dodecyl sulfate (SDS, $CH_3(CH_2)_{11}OSO_3Na$, 98.5%) and phosphoric acid (H_3PO_4, 85%) were all from Sigma-Aldrich, USA. 4-Mercapto-1-butanol ($HS(CH_2)_4OH$, ≥ 94%), and 8-mercapto-1-octanol ($HS(CH_2)_8OH$, 98%) were from Santa Cruz Biotechnology, Inc. Nitric acid (HNO_3, 70%) was from Fisher Scientific, UK. 100 mM McIlvaine buffer solution was prepared by mixing solutions of citric acid and Na_2HPO_4, with pH adjusted to 5.5. All chemicals were used as received and all solutions prepared with Millipore water (18.2 MΩ cm).

2.2. Preparation of FDH modified bioelectrodes

Prior to modification, the treatments of Au(111) and NPG are different but with the same purpose of creating clean surfaces, see Supplementary Materials. Au(111) electrodes were quenched using Millipore water saturated with hydrogen gas. NPG electrodes were prepared by the dealloying method and further activated in H_2SO_4 solution. Quenched Au(111) electrodes or activated NPG electrodes were then immersed into aqueous 3 mM MEA, BME, MPA or PPT for about 20 h to form SAMs on the gold electrodes. SAMs with variable-length thiols were formed by immersing quenched Au(111)-electrodes in 3 mM $HS(CH_2)_nOH$ (n = 2–4, 6, 8, 9, 11) ethanol solutions for 20 h. After soaking, the SAM functionalized electrodes were rinsed several times with ethanol and Millipore water. SAM modified Au(111) and NPG electrodes were then immersed in either 80 µL 1.5 mg mL^{-1} or 600 µL 0.6 mg mL^{-1} FDH solution in 100 mM pH5.5 McIlvaine buffer, respectively, at 4 °C for about 20 h.

2.3. Electrochemical characterization

Electrochemical testing was carried out using an Autolab PGSTAT12 instrument (Eco Chemie, Switzerland) with a three-electrode system. The FDH bioelectrode, a Pt wire, and a Ag/AgCl electrode were the working, counter, and reference electrode, respectively. CV and linear sweep voltammetry (LSV) of FDH modified electrodes in 100 mM pH 5.5 McIlvaine buffer were recorded at room temperature (ca. 20 °C) in the presence and absence of 100 mM fructose. The operational stability of the bioelectrodes was tested by chronoamperometry at 0.4 V for 7 days. All electrolytes were purged with argon gas for at least 30 min and an argon atmosphere maintained during electrochemical measurements. All potentials are referred to Ag/AgCl (sat. KCl). The current densities of the FDH modified NPG electrodes were calculated based on the geometric surface area of NPG, unless otherwise stated.

2.4. Assay of enzyme activity

50 mL Fe(III) sulfate-SDS buffer/McIlvaine buffer was prepared from 2.5 g Fe(III) sulfate, 1.5 g SDS and 4.75 mL H_3PO_4. The FDH modified electrodes were immersed in a mixture of McIlvaine buffer containing 0.1% Triton X-100 (0.7 mL) and 0.5 M fructose/McIlvaine buffer (0.2 mL), and equilibrated at 37 °C for 5 min. 0.1 M $K_3[Fe(CN)_6]$/0.1 M McIlvaine buffer (0.1 mL) was then added to the mixture. After 10 min, Fe(III) sulfate-SDS buffer/McIlvaine buffer (0.5 mL) was added to the mixture to quench the biocatalytic reaction as SDS serves as an inhibitor of FDH, and further incubated for 20 min to form a stable suspension of Prussian blue, Eq. (S1-3) [30]. The absorbance of the final solution at 660 nm was measured using a UV-2401PC UV-vis spectrophotometer (SHIMADZU, Japan). A linear calibration curve showing the relationship between known FDH concentration in solution and absorbance change was used to estimate the amount of immobilized active FDH on the electrode. This is based on the assumption that (i) the enzymatic activity of the immobilized FDH is the same as for free FDH in solution and (ii) the diffusion of fructose and $K_3[Fe(CN)_6]$ is fast. The assumption that the enzyme has the same activity in immobilized and free form in solution only applies, when the enzyme assay method is used to determine the trend in surface coverage on differently modified electrodes [8].

2.5. Numerical fitting to the polarization curves

Our numerical fitting to the electrocatalytic data is based on the model of Armstrong and associates [31] as exploited further by Xia and associates [27,32]. In this model a generic distribution function for the combined protein orientation and distance between the planar Au-electrode surface and the nearest enzyme redox center (here heme 2*c*) is introduced. A real distribution function for the inhomogeneous, anisotropic, and multi-dimensional electrode/SAM/FDH/solution interface would be extremely complex and way out of quantitative interpretation of real data. In Armstrong and associates' model this complexity was reduced to a rectangular distribution in the sense that interfacial ET is feasible within a distance/orientation range from the most (d_{min}) to the least (d_{max}) favourable configuration, where d is a coarse-grained representation of both distance and orientation. Within this range the interfacial ET rate constants at the most $k(d_{min})$ and least $k(d_{max})$ favourable configuration are taken to be correlated as $k(d_{max})/\ k(d_{min}) = exp(-\beta\Delta d)$, $\Delta d = d_{min}\text{-}d_{max}$. β ($Å^{-1}$) is a coarse-grained tunneling decay factor for ET through the combined SAM/intraprotein matter, here taken as 1.4 $Å^{-1}$ representative solely of the protein [27]. $\beta\Delta d$ is thus a core parameter in the data analysis. The smaller $\beta\Delta d$ the narrower the distribution and the better defined the productive configuration.

Armstrong and associates' model is represented by [27,31,32]

$$j_{lim,det} = n_s F k_c \Gamma_{det} \tag{1}$$

$$j = \frac{j_{lim}}{\beta \times \Delta d \times \left(1 + exp\left(\frac{n_E F}{RT} \times \left(E - E_E^{o'}\right)\right)\right)} \times ln\left|\frac{\left(1 + \exp\left(\frac{n_E F}{RT} \times \left(E - E_E^{o'}\right)\right)\right) + \frac{k_c}{k_{max}^o} \times exp\left(\frac{\alpha n_E F}{RT} \times \left(E - E_E^{o'}\right)\right)}{\exp\left(-\beta \times \Delta d\right) \times \left(1 + \exp\left(\frac{n_E F}{RT} \times \left(E - E_E^{o'}\right)\right)\right) + \frac{k_c}{k_{max}^o} \times exp\left(\frac{\alpha n_E F}{RT} \times \left(E - E_E^{o'}\right)\right)}\right| \tag{2}$$

where $j_{lim,det}$ is the limiting current density of a DET process (mA cm^{-2}), n_s the number of electrons in the substrate oxidation (2 for fructose oxidation catalyzed by FDH), F the Faraday constant (96,485 C mol^{-1}), and k_c the catalytic constant of FDH, which is in a range of 200–700 s^{-1} [12,33]. Γ_{det} is the surface concentration of the DET-effective enzymes on the electrode (mol cm^{-2}), n_E

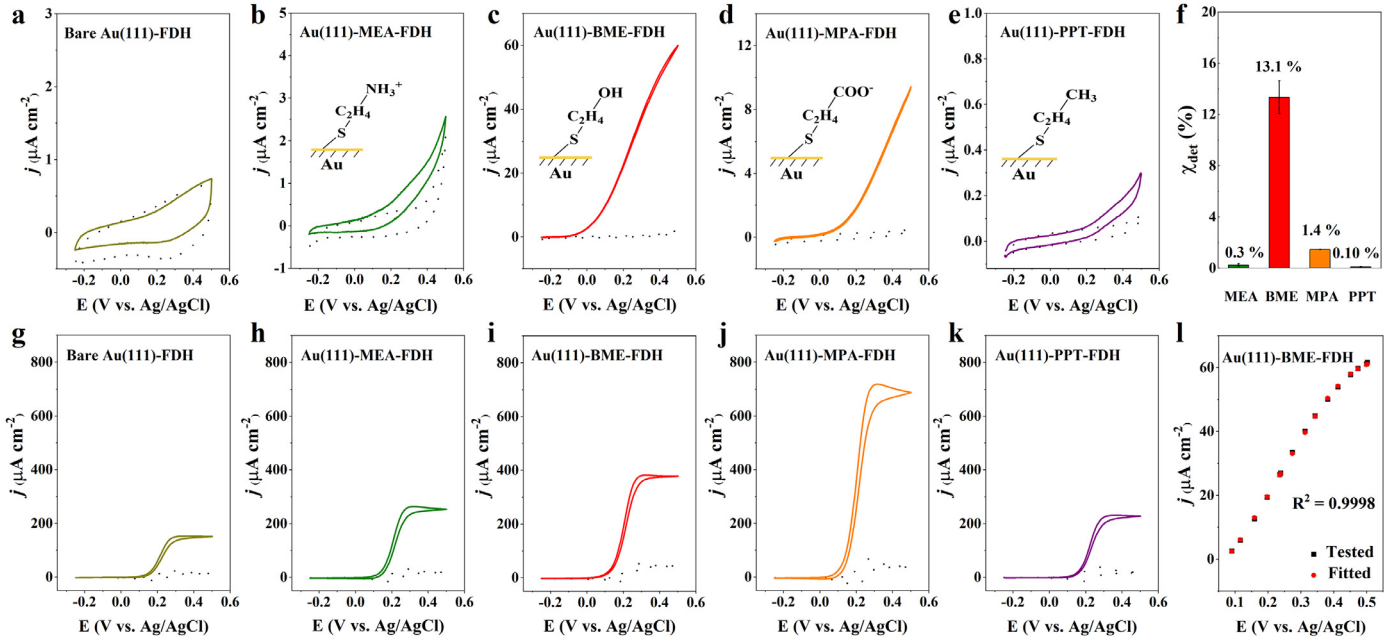

Fig. 1. DET (a–e) and MET (g–k) voltammograms of FDH based bioelectrodes on Au(111) in 100 mM McIlvaine buffer, pH 5.5 without (a–e) and with (g–k) 0.5 mM FcMeOH in the absence (dashed lines) and presence (solid lines) of 100 mM fructose. Scan rate 5 mV s^{-1}. (f) Fraction (χ_{det}) of FDH capable of DET on Au(111) with different SAMs. (l) The recorded and fitted polarization curves of Au(111)-BME-FDH in the presence of 100 mM fructose, $R^2 = 0.9998$.

the number of electrons in the rate-determining step of the interfacial ET process (1 in this system for heme), R the gas constant (8.314 J mol^{-1} K^{-1}), and T the absolute temperature (298 K). k^0_{max} is finally the standard electrochemical rate constant for optimally orientated FDH on the surface (s^{-1}), α the transfer coefficient (here taken as 0.5), and $E^{o'}$ the formal potential of heme 3*c* of FDH (-0.01 V) for electrochemical communication with the electrode surface [15,32]. Fitting was conducted using Microsoft Excel and is simplified by assembling different parameters, such as k_c/k^0_{max}, $\beta\Delta d$ and $k_c\Gamma_{det}$.

2.6. Homology modeling/docking of FDH

Subunits I and II of FDH were built using the online homology-modeling server, SWISS-MODEL (https://swissmodel.expasy.org/) [34]. Based on the sequence coverage and identity, the best templates suggested by the SWISS-MODEL are glucose dehydrogenase from Burkholderia cepacia (PDB: 6A2U) and thiosulfate dehydrogenase from Marichromatium purpuratum (PDB: 5LO9), respectively. The two subunits were docked together using the HADDOCK webserver (https://haddock.science.uu.nl/) in the distance constraints mode [35]. The surface charge distribution of FDH at pH 5.5 was generated with PyMol (Schrödinger, USA) assisted by the PDB2PQR web server [36].

3. Results and discussion

3.1. FDH voltammetry on Au(111)-electrodes modified by differently terminated SAMs

Au(111) electrodes with atomically planar surfaces are an ideal platform to investigate the effects of SAMs with variable terminal groups on the DET behaviour of FDH, *i.e.* -NH_2 (MEA), -OH (BME), -COOH (MPA) and -CH_3 (PPT) (Fig. S1). MEA, BME and MPA SAMs give hydrophilic electrode surfaces, while PPT and bare Au(111) surfaces are hydrophobic/non-polar. MEA gives a positively charged surface at pH 5.5 due to the formation of -NH_3^+, whereas the MPA surface is negatively charged. There would be no significant surface charges for BME and PPT modified Au(111). Table S1 shows the pKa values and charges of the thiols, indicating that the charge of the surface is determined by the terminal SAM groups rather than by the Au-S unit [37,38]. CVs of FDH on functionalized alkanethiol modified Au(111) electrodes in the potential range from -0.25 to 0.5 V were recorded with a relatively low scan rate of 5 mV s^{-1}. There are no visible redox waves from CVs in the range -0.2–0.5 V vs. Ag/AgCl in the absence of fructose (Fig. 1a–e). Differential pulse voltammetry (DPV) gives two pairs of redox peaks, possibly assigned to the FAD group (-0.27 V) and the Au(111) electrode (Fig. S2) [12], but no obvious redox peaks from the three heme groups can be observed in the range -0.1–0.2 V. The peaks around 0.2–0.4 V vs. Ag/AgCl are likely to be attributed to the complex adsorption and desorption of ions in the buffer solution [39,40]. The current density drastically increases on BME and MPA SAMs in the presence of 100 mM fructose, indicative of successful immobilization of active FDH and rapid DET between SAM modified Au(111) and FDH. Specifically, Au(111)-BME-FDH reaches a background-corrected maximum current density ($\Delta j_{max,det}$) of 55 ± 3 μA cm^{-2} (Fig. 1c, Table 1). There is, strictly speaking, no precise definition of the onset potential for bioelectrocatalysis [41]. Here we obtained the onset potentials by comparing the CVs of the bioelectrode in the presence and absence of fructose [4,42]. $E_{onset,det}$ for Au(111)-BME-FDH is about -0.12 V, consistent with reported $E^{o'}$ of heme 3*c* in FDH (Scheme 1) [25,27]. $\Delta j_{max,det}$ on different SAM modified Au(111) varies greatly, and follows the sequence: BME > MPA > MEA > PPT (Fig. 1a–e) [21]. In comparison, the DET response on bare Au(111) is negligible. The recorded Δj_{max} values at the potential of 0.5 V are summarized in Table 1.

The two most important FDH electrocatalytic parameters on the differently terminated SAMs are the catalytic rate constant, k_c (s^{-1}) and the FDH coverage in both productive DET configuration, Γ_{det} and in total, Γ (both in mol cm^{-2}). We shall take k_c to be the same at all the SAM-modified electrodes, both here and in the discussion of FDH electroactivity at variable-length alkanethiol modified electrodes, Section 3.4. This assumption is warranted by the noncovalent, i.e. relatively weak interaction between immobilized FDH and the considerable distance between FDH and the underly-

Table 1
Catalytic and kinetic constants of DET fructose oxidation catalysed by FDH on SAM modified Au(111) obtained from fitting of Eqs. (1) and (2).

Electrode	$E_{onset,det}$ (V vs. Ag/AgCl)	$\Delta j_{max,det}$(μA cm^{-2})	$E_{onset,met}$ (V vs. Ag/AgCl)	$\Delta j_{max,met}$(μA cm^{-2})	k_c/k^0_{max}	$k_c\Gamma_{det}$(mol cm^{-2} s^{-1})	$\beta\Delta d$
Bare Au(111)-FDH	–	–	0.08	144 ± 6	–	–	–
Au(111)-MEA-FDH	0.06	0.6 ± 0.2	0.07	239 ± 4	37 ± 0.8	(3.65 ± 0.28) × 10^{-11}	13.6 ± 0.1
Au(111)-BME-FDH	-0.12	55 ± 3	0.02	420 ± 4	4.3 ± 0.1	(5.22 ± 0.02) × 10^{-10}	7.4 ± 0.1
Au(111)-MPA-FDH	0.03	9.1 ± 0.2	0.05	641 ± 8	24 ± 0.5	(2.13 ± 0.02) × 10^{-10}	12.6 ± 0.1
Au(111)-PPT-FDH	0.14	0.2 ± 0.03	0.08	214 ± 4	3.1 ± 0.2	(4.13 ± 0.06) × 10^{-12}	13.6 ± 0.1

ing Au(111) or NPG electrode surfaces. This gentle reservation enables extracting the crucial mechanistic information about the FDH electrocatalysis, which would have been beyond reach if varying k_c values at all the different surfaces were invoked. Neither are varying k_c values warranted by the character of the bioelectrocatalytic data.

The DET limiting current densities ($j_{lim,det}$) for the electrodes are then directly determined by the amount of FDH in proper orientation (Γ_{det}) (Eq. (1)). A way to characterize the bioelectrode process further is to roughly estimate the total active enzyme loading (Γ), consisting of both DET-capable FDH and FDH still active but in an orientation unsuitable for DET. Saturation MET current density discloses the total amount of active FDH irrespective of orientation [4].

Herein, we adapt a core parameter (χ_{det}, obtained as the ratio of DET/MET current density) to justify the DET capability [43].

The MET reaction was characterized by CVs in McIlvaine buffer containing 0.5 mM FcMeOH in the absence or presence of 100 mM fructose at 5 mV s^{-1} (Fig. 1g–k). To ascertain that MET addresses all active enzyme, the mediator should be chosen with a large enough overpotential to minimize diffusion constraints in the access to immobilized FDH enzyme [4]. With this in mind, FcMeOH was selected as a mediator, with the further view that it is electrostatically neutral in one oxidation state and only singly charged in the second oxidation state (Eq. (S4-5)). FcMeOH with high concentration was dissolved in the buffer solution during experiments, leading to a insignificant mass transport control at the interface [44]. In the absence of fructose, FcMeOH undergoes a fast faradic reaction (Fig. 1g–k), and shows a pair of well-defined redox peaks with a peak separation (ΔE_p) of ca. 0.07 V and a mid-point potential ($E_{1/2}$) of ca. 0.23 V vs. Ag/AgCl (Table S2). FcMeOH can exchange electrons with electrode surfaces either directly through pinholes in the short-thiol SAMs or by electron tunneling through the short carbon chains [40]. Sigmoidal CVs, typical for electrocatalytic reactions undergoing MET [45], were obtained in the presence of fructose, with FcMeOH as the electron donor, and an $E_{onset,met}$ of 0.02 V for Au(111)-BME-FDH, which is higher than $E^{o'}$ of heme 3*c* (-0.01 V). This indicates that the MET pathway is likely to bypass the internal hemes and only the FAD cofactor and external FcMeOH mediator are involved (Scheme 1) [15].

MET Δj_{max} on different SAM modified Au(111) electrodes follows the sequence: MPA > BME > MEA > PPT > bare Au(111) (Table 1). Comparison between DET and MET at the same bioelectrode offers several observations. Although exhibiting negligible DET, which can be explained by the unfavourable enzyme orientation (Fig. 1a), FDH on the hydrophobic bare Au(111), still retains structural integrity and activity with a reasonable MET $\Delta j_{max,met}$ of 144 ± 6 μA cm^{-2} (Fig. 1g, Table 1). DET Δj_{max} of Au(111)-BME-FDH is the highest among all the Au(111) SAMs, and nearly six times higher than for Au(111)-MPA-FDH. Au(111)-MPA-FDH exhibits, however, the highest MET Δj_{max} of 641 ± 8 μA cm^{-2} (Fig. 1j, Table 1) which is reasonable, as the negatively charged surface can adsorb the largest amount of overall positively charged FDH (IEP: 6.59) [5]. Au(111)-MEA with positively charged surfaces is fraught with strong electrostatic repulsion with smaller FDH MET $\Delta j_{max,met}$. DET signals are also small, but still higher than those on Au(111)-PPT-FDH with a hydrophobic surface. The DET-capable fraction χ_{det} (Fig. 1f) is proposed here to crudely reflect the surface coverages of DET-capable enzyme relative to the total amount of immobilized active FDH [46,47]. χ_{det} on different SAM modified Au(111)-surfaces retains the same sequence as for DET $\Delta j_{max,det}$, i.e. BME > MPA > MEA > PPT. Au(111)-BME-FDH with the highest χ_{det} of ca. 13.1%, shows that the hydrophilic hydroxyl groups favour the largest ratio of FDH in optimum orientation among all the short thiols. This is consistent with previous reports showing that OH-terminated SAMs are the most favourable for DET of FDH [26,48]. However, there is certainly room for improvement [49], as all χ_{det} are still below 20%.

3.2. Structural homology modeling

The catalytic and ET subunits of FDH were assembled using homology modeling and structural docking, in order to visualize the interfaces and protein surface properties (Fig. 2). The electrostatic surface distribution at pH 5.5 shows that a large part of the surface is positively charged (Fig. 2a), consistent with the IEP of 6.59 [22]. A negatively charged thiol such as MPA would enable high FDH loading and a large MET $\Delta j_{max,met}$. We have previously seen a related pattern for ferredoxin, a strongly negatively charged protein but with a positively charged "hole" that seems to prevail on ferredoxin binding to MPA on Au(111) [50]. In contrast, positively charged MEA gives a low FDH loading and a small MET $\Delta j_{max,met}$. The protein surface in the proximity of heme 2*c*, assumed to be the FDH electron outlet (Scheme 1), does not bear a significant positive charge. This may explain why χ_{det} on Au(111)-MPA-FDH is not the highest among all the thiols. Negatively charged MPA may interact with FDH in a range of orientations, but not necessarily close to heme 2*c* for rapid DET.

Electrostatic surface mapping also identifies the distribution of polar/hydrophilic amino acid residues, which shows an overall quite hydrophilic surface with both positive and negative charges somewhat scattered in the heme 2*c* outlet area (Fig. 2a). This may explain why low enzyme loading is achieved on the hydrophobic bare Au(111) and PPT. The non-polar/hydrophobic and aromatic (Phe, Trp) amino acid residues are highlighted to directly visualize the hydrophobic regions of the FDH surface, (Fig. 2b). Most hydrophobic patches are in fact located close to the hemes, indicating a favourable CHR of the subunit II attachment site to the transmembrane unit. The surface structure around heme 2*c* is, however, subtle, with a mixture of hydrophobic and hydrophilic features. Although the DET mechanism is still not entirely clear, the moderately hydrophilic BME with the –OH terminal group is proven to be the most suitable thiol for DET of FDH and seems to accord roughly with the FDH surface structure around the critical site for electron inlet and outlet. Somewhat related composite patterns were reported for the multi-copper enzyme copper nitrite reductase (*Achromobacter xylosoxidans*) on Au(111)-electrodes modified by a variety of differently charged thiol-based SAMs [51].

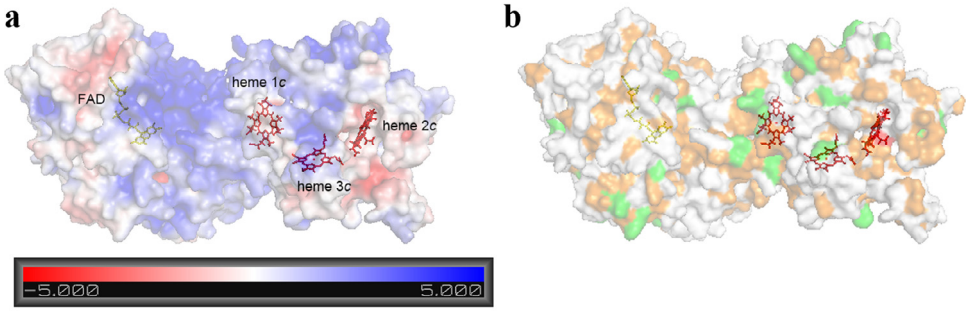

Fig. 2. (a) Surface charge distribution of FDH (homology model) at pH5.5 with blue and red color symbolizing positive and negative charges, respectively. (b) Molecular surface of FDH (homology model) with hydrophobic aliphatic amino acid residues highlighted in orange, hydrophobic aromatic amino acids (Phe, Trp) in green, and the remaining hydrophilic amino acids in white.

3.3. Numerical fitting of Eqs. (1) and (2) to the recorded polarization curves

Non-linear regression analysis was used to fit Eqs.(1) and (2) to the recorded LSV curves with a high confidence level, Figs. 1l, S3. k_c/k^0_{max}, $k_c\Gamma_{det}$ and $\beta\Delta d$ are the variable parameters [27,32,52]. As noted, the interfacial DET rate distribution is controlled by the variable distance between the electrode surface and the heme 2*c* group, and the enzyme surface orientation overall represented by the parameter combination $\beta\Delta d$. Au(111)-BME-FDH exhibits by far the lowest $\beta\Delta d$ (7.4 ± 0.1) among the SAMs, Table 1. Taking β = 1.4 Å^{-1} as an average among common values for covalent, hydrogen bond and through-space contacts [27], gives $\Delta d \approx$ 5.3 ± 0.1 Å. This value reflects the difference between the least and most productive limits of distance and orientation and therefore, how well the active enzyme surface is configured. Au(111)-BME-FDH also shows the largest $k_c\Gamma_{det}$ ((5.22 ± 0.02) × 10^{-10} mol cm^{-2} s^{-1}), reflecting the optimum surface properties for the highest loading of DET-capable FDH, still with the assumption that k_c on the different electrodes is the same for all the SAMs. $k_c\Gamma_{det}$ on different electrodes follows the same sequence as the DET current, $\Delta j_{max,det}$, i.e.: BME > MPA > MEA > PPT. k_c/k^0_{max} for Au(111)-BME-FDH is much smaller than for Au(111)-MPA-FDH and Au(111)-MEA-FDH, consistent with the most favorably configured heme 2*c* active site relative to the electrode surface. The trend for Au(111)-PPT-FDH and bare Au(111)-FDH was different. This could be associated with the non-negligible errors in the very low DET $\Delta j_{max,det}$. Overall, χ_{det} and $\beta\Delta d$ therefore emerge as highly useful parameters for evaluating an electrode surface for efficient DET, as further substantiated by our analysis of FDH electrocatalysis at variable length HS(CH$_2$)$_2$OH SAM modified Au(111) electrodes, Section 3.4. As the SAMs most favorable for productive DET, HS(CH$_2$)$_2$OH SAMs terminated with the hydroxyl group were therefore used in our further study.

3.4. FDH on Au(111) modified with variable-length HS(CH$_2$)$_n$OH SAMs

Au(111)-S(CH$_2$)$_n$OH-FDH bioelectrodes, where *n* is the number of methylene groups (*n* = 2–4, 6, 8, 9, 11), were prepared to investigate the effect of alkyl chain length on the enzyme DET reaction. With some reservations as to data scattering, catalytic current densities of FDH on Au(111)-S(CH$_2$)$_n$OH electrodes decrease approximately exponentially, with increasing number of -CH$_2$ groups, Fig. 3a. The slope, ≈ 1 Å^{-1} is informative, as this value points to electron tunneling through the alkanethiol SAM as rate determining in the overall two-step electrocatalytic FDH process, in which the catalytic process (k_c) itself is the second step, cf. below. This is in contrast to our recent study of the electrocatalytic activity of Prussian blue nanoparticles on variable length alkanethiols [53,54]. Much smaller decay factors (<< 1.0 n^{-1}) were here observed, indicative that the electron tunneling step and the catalytic process jointly control the overall two-step process.

Au(111)-S(CH$_2$)$_3$OH-FDH exhibits a DET $\Delta j_{max,det}$ of 34 ± 4 μA cm^{-2}, which is only 60% that on Au(111)-S(CH$_2$)$_2$OH-FDH, but more than ten times smaller when *n* is 6, 8, 9 and 11 (Figs. 3a, S6a). We have reported similar -CH$_2$ number dependent DET behaviour for laccase [55] and the blue copper ET protein azurin [56]. Notably, $E_{onset,det}$ is close to -0.12 V with short SAMs (*n* = 2, 3), but greatly increased to 0.14 V for long SAM molecules. The shift cannot only be associated with the tunneling distance but must also involve structural reorganization in the local microenvironment. Similar effects are reported for simple redox proteins, e.g. the blue copper protein azurin [56].

Fig. S4 depicts the non-linear fitting results of Au(111)-S(CH$_2$)$_n$OH-FDH bioelectrodes. Fig. 3c and 3e prompt two other observations. Although based on a restricted distance range, *n* = 2–9, or an interfacial electron transfer distance variation of ≈ 1 nm, Fig. 3c does indicate a dual distance behavior, with approximately exponential distance dependence at "long" distances, ≥ ½ nm and a trend towards distance independence at distances shorter than ≈ ½ nm. This pattern follows other protein or biomimetic protein patterns, for example the blue copper protein azurin adsorbed on variable length alkanethiols [56] and molecular scale Prussian blue nanoparticles adsorbed on variable length and variably terminated alkanethiols [53,54]. A first rationale is that the dual distance behavior reflects a transition from strongly distance dependent diabatic ET with weak electrode/enzyme interactions at long distances to the distance independent adiabatic limit of strong interactions at short distances. Other rationales have also been forwarded [56].

Fig. 3e discloses another DET feature of FDH behavior on variable length HS(CH$_2$)$_n$OH SAMs. $\beta\Delta d$ depends approximately linearly on *n* at short or intermediate distances with $\beta\Delta d$ values in the range 8–10. At longer distances $\beta\Delta d$ approaches the constant, larger value of ≈ 12, Table 2. With β in the range 1.0–1.4 Å^{-1}, Δd values in the range 7–10 Å and 9–12 Å, respectively, emerge. With a view of the physical meaning of Δd as a distance *range*, within which interfacial FDH electrocatalysis is feasible, *i.e.* $\Delta d = d_{min}$-d_{max}, this observation suggests that the distance/orientation distribution is relatively narrow for the short SAM linkers, but wider and approaching a stable value for the longer SAM linkers. This implies in turn that FDH is bound (relatively) rigidly on the short-linker SAMs but in "softer", configurationally flexible patterns on the SAMs of longer linker molecules. As noted, repulsive image forces induced in the dielectric SAM by the local surface charges in the enzyme would increase and rationalize the decreased coverage with increasing thiol length [57]. This can be compared with reports on DET of *Streptomyces coelicolor* laccase and *P. stutzeri* cytochrome c_4 on variable length thiol SAMs [55,58].

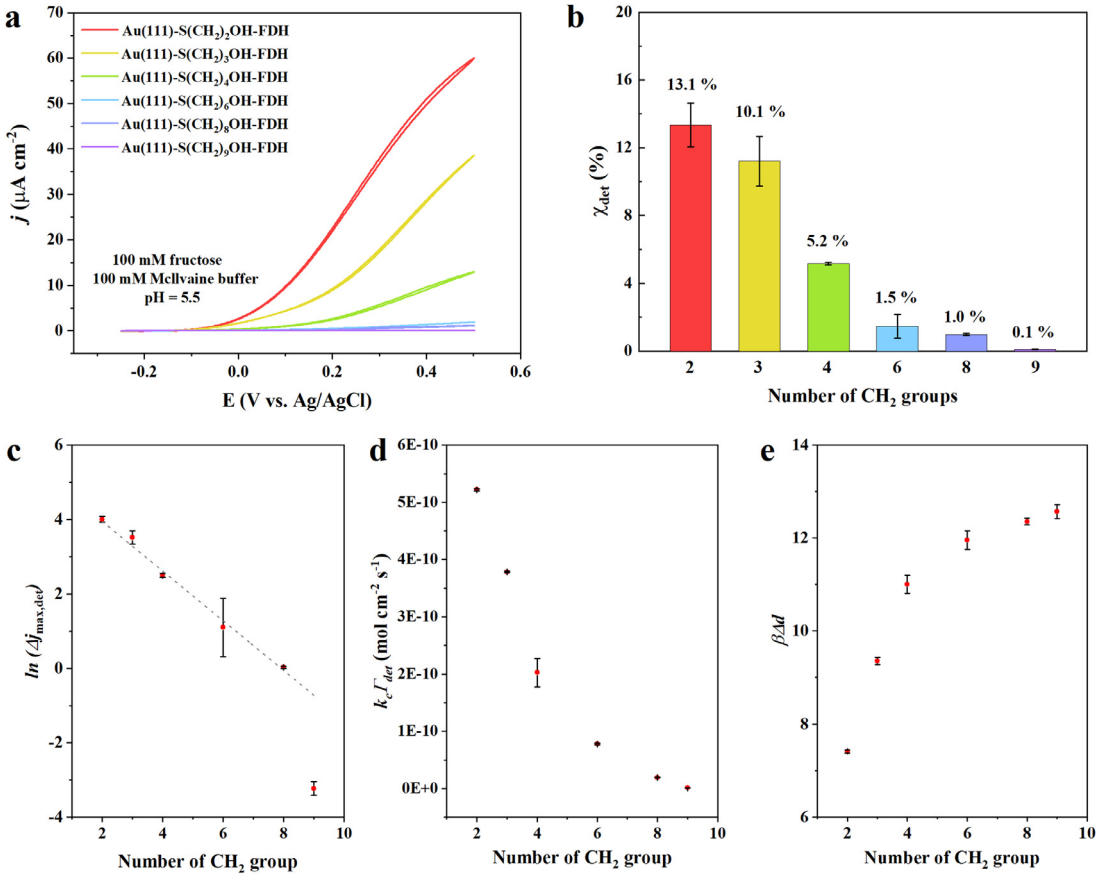

Fig. 3. CVs of FDH on Au(111) modified with variable-length $HS(CH_2)_nOH$ SAMs (n = 2, 3, 4, 6, 8, 9) in 100 mM pH 5.5 McIlvaine buffer containing 100 mM fructose. Scan rate 5 mV s^{-1}. (b) χ_{det} of FDH on Au(111) electrodes with $HS(CH_2)_nOH$ SAMs (n = 2, 3, –4, 6, 8, 9). The correlation of (c) $ln(\Delta j_{max,det})$, (d) $k_c\Gamma_{det}$ and (e) $\beta\Delta d$ with the ET distance represented as the number of methylene groups in the SAMs (The straight line in Fig. 3c is a guide for the eye).

Table 2
Catalytic and kinetic constants of DET-type fructose oxidation of FDH modified Au(111) electrodes with variable-length $HS(CH_2)_nOH$ SAMs.

Electrode	$E_{onset,det}$ (V vs. Ag/AgCl)	$\Delta j_{max,det}$(μA cm^{-2})	$E_{onset,met}$ (V vs. Ag/AgCl)	$\Delta j_{max,met}$(μA cm^{-2})	k_c/k^0_{max}	$k_c\Gamma_{det}$(mol cm^{-2} s^{-1})	$\beta\Delta d$
Au(111)-$S(CH_2)_2$OH-FDH	-0.12	55 ± 3	0.02	420 ± 4	4.3 ± 0.1	(5.22 ± 0.02) × 10^{-10}	7.4 ± 0.1
Au(111)-$S(CH_2)_3$OH-FDH	-0.12	34 ± 4	0.03	337 ± 3	8.7 ± 0.1	(3.78 ± 0.01) × 10^{-10}	9.4 ± 0.1
Au(111)-$S(CH_2)_4$OH-FDH	-0.10	13 ± 1	0.05	237 ± 9	16.5 ± 4.9	(2.03 ± 0.25) × 10^{-10}	11.0 ± 0.2
Au(111)-$S(CH_2)_6$OH-FDH	-0.10	3.5 ± 1.5	0.05	238 ± 10	8.6 ± 0.3	(7.79 ± 0.10) × 10^{-11}	11.9 ± 0.2
Au(111)-$S(CH_2)_8$OH-FDH	-0.03	1.03 ± 0.03	0.06	105 ± 4	18.2 ± 1.3	(1.95 ± 0.01) × 10^{-11}	12.4 ± 0.1
Au(111)-$S(CH_2)_9$OH-FDH	0.14	0.04 ± 0.01	0.16	37 ± 3	2.5 ± 0.1	(1.20 ± 0.01) × 10^{-12}	12.6 ± 0.1

The MET-type bioelectrocatalysis of Au(111)-$S(CH_2)_n$OH-FDH (n = 2, 3, –4, 6, 8, 9, 11) was also recorded (Figs. S5, S6b). In the blank CVs, FcMeOH exhibits quasi-reversible voltammetry with a similar ΔE_p and $E_{1/2}$ on short chain SAMs (n = 2, 3, –4, 6, 8), in contrast to irreversible behaviour for long chain SAMs (n = 9, 11) with a wider ΔE_p and asymmetric anodic/cathodic current densities (Table S2). It is known that long carbon chain thiols result in denser SAMs, leaving fewer or no vacancies [59]. FcMeOH can then only exchange electrons with the electrode by tunneling through long chain SAMs. In the presence of fructose, MET $\Delta j_{max,met}$ still drastically decreases from 420 ± 4 μA cm^{-2} on Au(111)-$S(CH_2)_2$OH-FDH to 37 ± 3 μA cm^{-2} on Au(111)-$S(CH_2)_9$OH-FDH. $E_{onset,met}$ also greatly increases when n = 9, implying higher overpotentials. Fig. 3b also shows that χ_{det} decreases notably with increasing n. χ_{det} of Au(111)-$S(CH_2)_{11}$OH-FDH was disregarded due to the poor DET and MET performance of this long-chain thiol SAM. As anticipated, these results show again that SAMs with short –$S(CH_2)_n$OH carbon chain lengths are most suitable for the DET of FDH.

However, MET $\Delta j_{max,met}$ is not directly correlated with the total amount of active FDH loading when n > 9, as the mediator cannot easily access the gold electrode for exchanging electrons in this length range. FDH loading (Γ) was instead measured by enzymatic assay in solution with $K_3[Fe(CN)_6]$ as no electron donor or interfacial ET involved. A linear relationship between the absorbance changes at 660 nm due to the formation of Prussian blue (Eq. S3) and the amount of FDH is shown in Fig. S7, and could be used as a calibration curve to estimate Γ (Table S3). The *trend* in the Γ variation is, however, more important than the *absolute* value of Γ assuming that the FDH activity is the same in immobilized and free forms [8]. Γ decreases with increasing thiol length, with a 10-fold decrease in Γ between Au(111)-$S(CH_2)_2$OH-FDH and Au(111)-$S(CH_2)_{11}$OH-FDH. This difference is, however, much smaller than for MET $\Delta j_{max,met}$ and shows that the poor MET $\Delta j_{max,met}$ on long thiol SAM based electrodes is mainly due to increasingly unfavorable electron tunneling, and not to enzyme loading.

The kinetic parameters obtained from fitting to the polarization curves of Au(111)-$S(CH_2)_n$OH-FDH electrodes, Fig. 3e are summa-

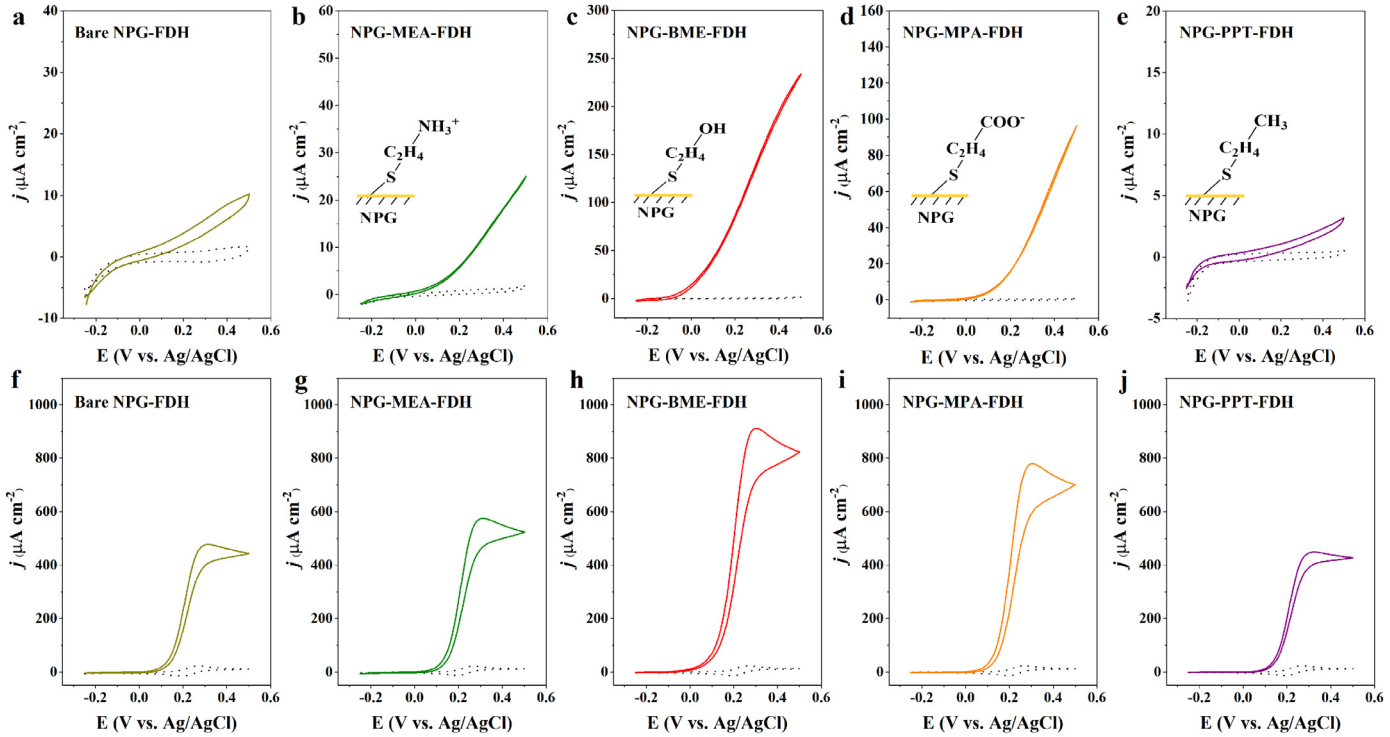

Fig. 4. (a–e) DET voltammograms of FDH on NPG electrodes modified with MEA, BME, MPA and PPT SAMs in 100 mM pH 5.5 McIlvaine buffer in the absence (dashed lines) and presence (solid lines) of 100 mM fructose. Scan rate: 5 mV s^{-1}. (f–j) MET FDH voltammograms of FDH on NPG modified with MEA, BME, MPA and PPT SAMs in 100 mM pH5.5 McIlvaine buffer with and without 0.5 mM FcMeOH, in the absence (dashed lines) and presence (solid lines) of 100 mM fructose. Scan rate 5 mV s^{-1}.

rized in Table 2. As noted, a lower $\beta\Delta d$ means a narrower distribution between most and least productive ET distance/orientation. $\beta\Delta d$ again increases conspicuously with increasing chain length, Fig. 3e resulting in broader FDH distance and orientation distributions. A constant value is reached at large distances (large values of n), where bound FDH is spatially far from the electrode surface and FDH electrocatalytic performance expected to stabilize.

Fig. 3d shows the relationship between $k_c\Gamma_{det}$ and SAM chain length, with a significantly downward trend with increasing number of CH_2 groups, pointing to notably but close to linearly decreasing FDH coverage as the alkanethiol length (SAM thickness) increases. As noted, the $\Delta j_{max,det}$ dependence on the number of CH_2 groups, Fig. 3c, depends, however, approximately exponentially, i.e. much more strongly on the alkanethiol chain length with a slope (≈ 1 $Å^{-1}$). This testifies to electron tunneling as the rate determining step in the overall two-step interfacial bioelectrocatalytic ET process.

3.5. FDH on bare and variably terminated SAM modified NPG electrodes

NPG materials with nanoporous structure have been studied as enzyme scaffolds for DET-type bioelectrocatalysis, Fig. 5a [28]. NPG is mostly prepared through a dealloying method. SEM images show a random nanoporous structure (Fig. S8a). NPG (thickness ca. 100 nm, average pore diameter 30 nm, R_f: 6.6, Fig. S8c) with a moderate pore size and relatively high surface area allowing the accommodation of FDH is used in this study [23]. CVs for FDH on variously terminated SAM functionalized NPG electrodes are shown in Fig. 4. As for Au(111) bioelectrodes, there are no clear redox waves associated with the heme groups in the absence of fructose. In the presence of 100 mM fructose, the DET current densities on NPG electrodes typically outperform those on Au(111) electrodes (Fig. 4a–e). The trend of thiol-dependent DET performance is the same as for Au(111), with NPG-BME-FDH exhibiting the largest DET $\Delta j_{max,det}$ of 238 ± 10 μA cm^{-2}, about four times that of Au(111)-BME-FDH. The calibration curve was obtained in long-term operation from blank to 200 mM over at least 4 h with an apparent K_M of 4.7 ± 0.2 mM (Fig. S9). Notably, a DET signal of FDH on bare NPG is observed as the addition of fructose causes visible catalytic oxidation currents, Fig. 4a. This is in contrast to FDH on bare Au(111), for which no distinguishable catalytic DET response of FDH on addition of fructose is apparent, Fig. 1a. All these results show clearly better DET performance of FDH on NPG than on Au(111), facilitated by the porous structure and large surface area of NPG, Fig. 5a [28].

MET-type catalytic performance of NPG based bioelectrodes is also superior to Au(111) electrodes, Fig. 4f–j, Table S4. NPG-BME-FDH exhibits again the highest MET $\Delta j_{max,met}$ of 846 ± 50 μA cm^{-2}, which is almost twice that on Au(111)-BME-FDH (420 ± 4 μA cm^{-2}, Table 1), and related to the higher Γ due to the nanoporous NPG architecture (Table S5). Γ on NPG-BME-FDH was found to be 1.34 × 10^{-9} mol cm^{-2}, approximately twice that for Au(111)-BME-FDH (6.48 × 10^{-10} mol cm^{-2}, Table S3). This is lower than the R_f value of 6.6, but a two-fold increase of Γ, is reasonable and consistent with a previous report [60] and clearly indicative that coverage and χ_{det} do not simply follow the electrode surface area but also depend on details of the Au-electrode surface structure. χ_{det} on NPG bioelectrodes also increases significantly compared to Au(111) (Fig. 5b), i.e. by a factor of 2 on NPG-BME-FDH (28%) and by a factor of 40 compared to bare NPG (2%).

Operational stability of Au(111)-BME-FDH, Au(111)-MPA-FDH, NPG-BME-FDH and NPG-MPA-FDH in the buffer containing 100 mM fructose at + 0.4 V over a period of seven days was addressed by chronoamperometry. Au(111)-BME-FDH and NPG-BME-FDH retain 14.5% and 46.2% of the initial current density, respectively, Fig. 6a, while Au(111)-MPA-FDH and NPG-MPA-FDH retain 10.5% and 25.4%, respectively, Fig. S11a. This means that FDH on hydrophilic SAM modified electrodes is typically quite stable, even though immobilized solely by physical interactions, believed to be

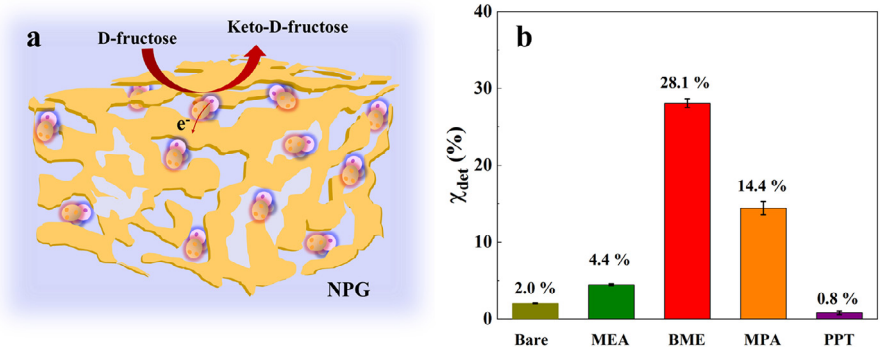

Fig. 5. (a) Schematic illustration of NPG for FDH loading. (b) χ_{det} of FDH on bare NPG and NPG modified with MEA, BME, MPA and PPT SAMs.

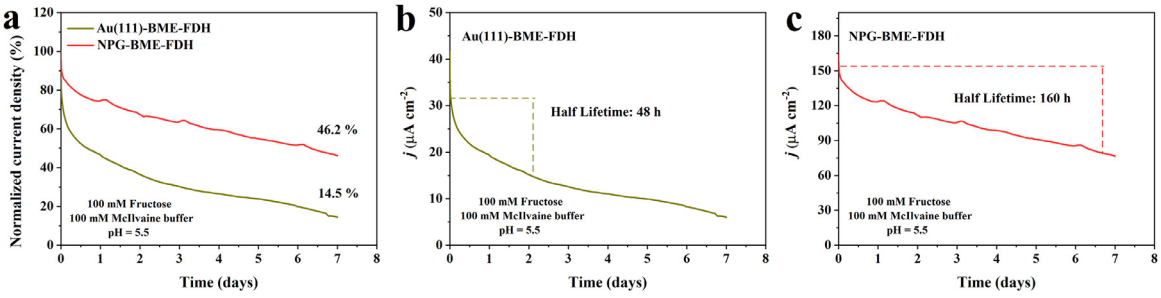

Fig. 6. The operational stability of FDH at + 0.4 V on Au(111) and NPG modified with BME.

relatively weak and not by covalent interactions. The real-time changes of current density of FDH on Au(111) and NPG electrodes are shown in Figs. 6b,c and S11b,c. FDH on modified NPG electrodes thus displays superior stability with the half-lifetime of 160 h (NPG-BME-FDH) and 123 h (NPG-MPA-FDG) compared with 48 h (Au(111)-BME-FDH) and 103 h (Au(111)-MPA-FDG).

As a comparison with the BME SAMs, the positively charged FDH is exposed to stronger electrostatic forces on the negatively charged MPA SAM, suggesting that the stability on the MPA SAM is higher than on the BME SAM, and with a longer half-lifetime on both Au(111) and NPG electrodes. The bioelectrode performance after the stability tests was also evaluated by CV (Figs. S10, S12). Au(111)-BME-FDH and Au(111)-MPA-FDH have basically lost all DET catalytic performance after the stability test, whereas NPG-BME-FDH and NPG-MPA-FDH retain, ca. 20% of the original catalytic current. Notably, Au(111)-BME-FDH and NPG-BME-FDH retain more than half their initial MET catalytic current, and Au(111)-MPA-FDH and NPG-MPA-FDH a quarter of the initial MET performance. This indicates that (i) the significant loss of DET signal on BME modified electrodes is not primarily by enzyme leakage [61,62]; (ii) much of the FDH is still active on the electrodes after long-time stability tests, whereas the optimal orientation is changed towards decreased DET performance. Overall, we can conclude that NPG: (i) improves the enzyme loading by its large surface area; (ii) notably facilitates DET activities of FDH; and (iii) significantly stabilizes the favorable orientations of FDH. These improved features are rooted in the confined porous structure. Physically they can be ascribed to better FDH organization and perhaps more favorable electronic FDH/SAM/NPG interactions compared with Au(111) (electronic transmission coefficients/tunnelling factors) [63].

4. Conclusion

Our primary overarching objectives in the present study were to map the bioelectrocatalysis of FDH as a biochemically and biotechnologically broadly important enzyme, in new molecular mechanistic detail. Our detailed study has progressed along two major lines with focus on the surface orientation and mechanistic detail of FDH in bioelectrochemical action on well-defined pure and SAM modified gold electrodes. One line was to map the effects of variably functionalized and variable-length thiol SAMs on Au(111) surfaces in FDH electrocatalysis. The other line was to compare the Au(111)-electrode with analogous pure and SAM-modified NPG electrodes.

Major outcomes are: (i) The DET-capable FDH fraction, χ_{det}, was mapped in detail and found to be useful for diagnosing the overall efficiency of the interfacial FDH electrochemical ET processes. (ii) A homology model of FDH was built and found to be highly beneficial to analyze the surface electrostatic field distribution and hydrophobic amino acid residue surface distribution around the heme 2*c* ET site. (iii) According with the computed FDH surface structure around heme 2*c*, the short hydrophilic but electrostatically neutral 2-mercaptoethanol (BME) SAM thiol was found to display by far the strongest DET electrocatalysis and largest χ_{det}. The crude but efficient fitting model was found to be informative and the $\beta\Delta d$ value obtained the smallest for BME, indicating more precisely controlled protein distance/orientation than for any other of the functionalized thiol SAMs tested. With the exception of negatively charged mercaptopropionic acid, MPA, all other SAMs exhibited much smaller FDH surface coverage and ET rates. (iv) The three core parameters for variable-length $HS(CH_2)_nOH$, *i.e.* DET active loading, Γ_{det}, DET-capable fraction, χ_{det}, and limiting $\Delta j_{max,det}$ all decrease strongly with increasing carbon chain length (n). $\beta\Delta d$ reflects increasing surface disorder or increasing conformational lability with increasing carbon chain length. The approximately exponential dependence of $\Delta j_{max,det}$ on n is as expected, and the decay constant, $\beta \approx 1.0\ n^{-1}$ is close to values often observed for tunneling through aliphatic thiol-based alkane linkers. This observation suggests that the electron tunneling step is core in the overall FDH catalysis with the electrocatalytic FDH conversion retained. (v) FDH on NPG follows broadly FDH on Au(111) regarding the catalytic efficiency of the variably functionalized thiol SAMs, again with BME as by far the most efficient. $\Delta j_{max,det}$ and $\Delta j_{max,met}$ on BME modified NPG are, however, several-fold higher than on

Au(111). In part this can be ascribed to higher enzyme loading, but more interestingly also to FDH orientation better suited for facile FDH interfacial bioelectrochemical ET and electrocatalysis. Furthermore, retaining operational stability over more than one week, as observed for FDH on NPG electrodes, would in fact ensure ample time for practical FDH/NPG use in biosensors and biofuel cells.

Declaration of Competing Interest

The authors declare that they have no known competing financial interests or personal relationships that could have appeared to influence the work reported in this paper.

Credit authorship contribution statement

Xiaomei Yan: Data curation, Methodology, Writing – original draft. **Su Ma:** Methodology. **Jing Tang:** Data curation. **David Tanner:** Writing – review & editing. **Jens Ulstrup:** Formal analysis, Writing – review & editing. **Xinxin Xiao:** Data curation, Methodology, Writing – review & editing. **Jingdong Zhang:** Methodology, Resources.

Acknowledgments

X.Y. acknowledges support from the China Scholarship Council (No. 201806650009). Financial support from The Danish Council for Independent Research for the YDUN project (DFF 4093-00297, to J.Z.), Villum Experiment (Grant No. 35844, to X.X.) and the Russian Science Foundation (project No 17-13-01274, to J.U.) is gratefully acknowledged. S.M. acknowledges funding from the Vienna Science and Technology Fund (WWTF-Project LS17-069).

Supplementary materials

Supplementary material associated with this article can be found, in the online version, at doi:10.1016/j.electacta.2021.138946.

References

[1] C.C. Moser, J.M. Keske, K. Warncke, R.S. Farid, P.L. Dutton, Nature of biological electron transfer, Nature 355 (1992) 796–802.
[2] J. Zhang, A.M. Kuznetsov, I.G. Medvedev, Q. Chi, T. Albrecht, P.S. Jensen, J. Ulstrup, Single-molecule electron transfer in electrochemical environments, Chem. Rev. 108 (2008) 2737–2791.
[3] K. Elouarzaki, D. Cheng, A.C. Fisher, J.M. Lee, Coupling orientation and mediation strategies for efficient electron transfer in hybrid biofuel cells, Nat. Energy 3 (2018) 574–581.
[4] X. Xiao, H. Xia, R. Wu, L. Bai, L. Yan, E. Magner, S. Cosnier, E. Lojou, Z. Zhu, A. Liu, Tackling the challenges of enzymatic (bio)fuel cells, Chem. Rev. 119 (2019) 9509–9558.
[5] T. Siepenkoetter, U. Salaj-Kosla, X. Xiao, P.Ó. Conghaile, M. Pita, R. Ludwig, E. Magner, Immobilization of redox enzymes on nanoporous gold electrodes: applications in biofuel cells, ChemPlusChem 82 (2017) 553–560.
[6] T. Adachi, Y. Kaida, Y. Kitazumi, O. Shirai, K. Kano, Bioelectrocatalytic performance of d-fructose dehydrogenase, Bioelectrochemistry 129 (2019) 1–9.
[7] S. Gentil, S.M. Che Mansor, H. Jamet, S. Cosnier, C. Cavazza, A. Le Goff, Oriented immobilization of [NiFeSe] hydrogenases on covalently and noncovalently functionalized carbon nanotubes for H_2/Air enzymatic fuel cells, ACS Catal. 8 (2018) 3957–3964.
[8] J. Tang, R.M.L. Werchmeister, L. Preda, W. Huang, Z. Zheng, S. Leimkühler, U. Wollenberger, X. Xiao, C. Engelbrekt, J. Ulstrup, J. Zhang, Three-dimensional sulfite oxidase bioanodes based on graphene functionalized carbon paper for sulfite/O_2 biofuel cells, ACS Catal. 9 (2019) 6543–6554.
[9] C. Vaz-Dominguez, S. Campuzano, O. Rüdiger, M. Pita, M. Gorbacheva, S. Shleev, V.M. Fernandez, A.L. De Lacey, Laccase electrode for direct electrocatalytic reduction of O_2 to H_2O with high-operational stability and resistance to chloride inhibition, Biosens. Bioelectron. 24 (2008) 531–537.
[10] T. Adachi, Y. Kitazumi, O. Shirai, K. Kano, Direct electron transfer-type bioelectrocatalysis of redox enzymes at nanostructured electrodes, Catalysts 10 (2020) 236.
[11] K. Murata, K. Kajiya, N. Nakamura, H. Ohno, Direct electrochemistry of bilirubin oxidase on three-dimensional gold nanoparticle electrodes and its application in a biofuel cell, Energy Environ. Sci. 2 (2009) 1280–1285.
[12] M. Kizling, R. Bilewicz, Fructose dehydrogenase electron transfer pathway in bioelectrocatalytic reactions, ChemElectroChem 5 (2018) 166–174.
[13] T. Miyake, S. Yoshino, T. Yamada, K. Hata, M. Nishizawa, Self-regulating enzyme–nanotube ensemble films and their application as flexible electrodes for biofuel cells, J. Am. Chem. Soc. 133 (2011) 5129–5134.
[14] P. Bollella, L. Gorton, R. Antiochia, Direct electron transfer of dehydrogenases for development of 3rd generation biosensors and enzymatic fuel cells, Sensors 18 (2018) 1319.
[15] S. Kawai, T. Yakushi, K. Matsushita, Y. Kitazumi, O. Shirai, K. Kano, The electron transfer pathway in direct electrochemical communication of fructose dehydrogenase with electrodes, Electrochem. Commun. 38 (2014) 28–31.
[16] Y. Hibino, S. Kawai, Y. Kitazumi, O. Shirai, K. Kano, Mutation of heme c axial ligands in d-fructose dehydrogenase for investigation of electron transfer pathways and reduction of overpotential in direct electron transfer-type bioelectrocatalysis, Electrochem. Commun. 67 (2016) 43–46.
[17] P. Bollella, Y. Hibino, K. Kano, L. Gorton, R. Antiochia, Enhanced direct electron transfer of fructose dehydrogenase rationally immobilized on a 2-Aminoanthracene diazonium cation grafted single-walled carbon nanotube based electrode, ACS Catal. 8 (2018) 10279–10289.
[18] Y. Sugimoto, S. Kawai, Y. Kitazumi, O. Shirai, K. Kano, Function of C-terminal hydrophobic region in fructose dehydrogenase, Electrochim. Acta 176 (2015) 976–981.
[19] M.T. Meredith, M. Minson, D. Hickey, K. Artyushkova, D.T. Glatzhofer, S.D. Minteer, Anthracene-modified multi-walled carbon nanotubes as direct electron transfer scaffolds for enzymatic oxygen reduction, ACS Catal. 1 (2011) 1683–1690.
[20] Y. Ogawa, Y. Takai, Y. Kato, H. Kai, T. Miyake, M. Nishizawa, Stretchable biofuel cell with enzyme-modified conductive textiles, Biosens. Bioelectron. 74 (2015) 947–952.
[21] M. Tominaga, C. Shirakihara, I. Taniguchi, Direct heterogeneous electron transfer reactions and molecular orientation of fructose dehydrogenase adsorbed onto pyrolytic graphite electrodes, J. Electroanal. Chem. 610 (2007) 1–8.
[22] P. Bollella, Y. Hibino, K. Kano, L. Gorton, R. Antiochia, Highly sensitive membraneless fructose biosensor based on fructose dehydrogenase immobilized onto aryl thiol modified highly porous gold electrode: characterization and application in food samples, Anal. Chem. 90 (2018) 12131–12136.
[23] T. Siepenkoetter, U. Salaj-Kosla, E. Magner, The immobilization of fructose dehydrogenase on nanoporous gold electrodes for the detection of fructose, ChemElectroChem 4 (2017) 905–912.
[24] X. Yan, J. Tang, D. Tanner, J. Ulstrup, X. Xiao, Direct electrochemical enzyme electron transfer on electrodes modified by self-assembled molecular monolayers, Catalysts 10 (2020) 1458.
[25] K. Murata, M. Suzuki, K. Kajiya, N. Nakamura, H. Ohno, High performance bioanode based on direct electron transfer of fructose dehydrogenase at gold nanoparticle-modified electrodes, Electrochem. Commun. 11 (2009) 668–671.
[26] S. Kawai, T. Yakushi, K. Matsushita, Y. Kitazumi, O. Shirai, K. Kano, Role of a non-ionic surfactant in direct electron transfer-type bioelectrocatalysis by fructose dehydrogenase, Electrochim. Acta 152 (2015) 19–24.
[27] H. Xia, Y. Hibino, Y. Kitazumi, O. Shirai, K. Kano, Interaction between d-fructose dehydrogenase and methoxy-substituent-functionalized carbon surface to increase productive orientations, Electrochim. Acta 218 (2016) 41–46.
[28] X. Xiao, P. Si, E. Magner, An overview of dealloyed nanoporous gold in bioelectrochemistry, Bioelectrochemistry 109 (2016) 117–126.
[29] H. Funabashi, K. Murata, S. Tsujimura, Effect of Pore size of MgO-templated carbon on the direct electrochemistry of D-fructose dehydrogenase, Electrochemistry 83 (2015) 372–375.
[30] M. Ameyama, E. Shinagawa, K. Matsushita, O. Adachi, D-fructose dehydrogenase of gluconobacter industrius: purification, characterization, and application to enzymatic microdetermination of D-fructose, J. Bacteriol. 145 (1981) 814–823.
[31] C. Léger, A.K. Jones, S.P.J. Albracht, F.A. Armstrong, Effect of a dispersion of interfacial electron transfer rates on steady state catalytic electron transport in [NiFe]-hydrogenase and other enzymes, J. Phys. Chem. B 106 (2002) 13058–13063.
[32] Y. Kaida, Y. Hibino, Y. Kitazumi, O. Shirai, K. Kano, Ultimate downsizing of d-fructose dehydrogenase for improving the performance of direct electron transfer-type bioelectrocatalysis, Electrochem. Commun. 98 (2019) 101–105.
[33] M. Kizling, M. Dzwonek, A. Więckowska, R. Bilewicz, Size does matter—mediation of electron transfer by gold clusters in bioelectrocatalysis, ChemCatChem 10 (2018) 1988–1992.
[34] A. Waterhouse, M. Bertoni, S. Bienert, G. Studer, G. Tauriello, R. Gumienny, F.T. Heer, T.A.P. de Beer, C. Rempfer, L. Bordoli, R. Lepore, T. Schwede, SWISS-MODEL: homology modeling of protein structures and complexes, Nucleic Acids Res. 46 (2018) W296–W303.
[35] G.C.P. van Zundert, J.P.G.L.M. Rodrigues, M. Trellet, C. Schmitz, P.L. Kastritis, E. Karaca, A.S.J. Melquiond, M. van Dijk, S.J. de Vries, A.M.J.J. Bonvin, The HADDOCK2.2 web server: user-friendly integrative modeling of biomolecular complexes, J. Mol. Biol. 428 (2016) 720–725.
[36] T.J. Dolinsky, J.E. Nielsen, J.A. McCammon, N.A. Baker, PDB2PQR: an automated pipeline for the setup of Poisson-Boltzmann electrostatics calculations, Nucleic Acids Res. 32 (2004) W665–W667.
[37] J.R. Reimers, M.J. Ford, S.M. Marcuccio, J. Ulstrup, N.S. Hush, Competition of van der Waals and chemical forces on gold-sulfur surfaces and nanoparticles, Nat. Rev. Chem. 1 (2017) 17.
[38] J.R. Reimers, M.J. Ford, A. Halder, J. Ulstrup, N.S. Hush, Gold surfaces and nanoparticles are protected by Au(0)-thiyl species and are destroyed when Au(I)-thiolates form, Proc. Natl. Acad. Sci. 113 (2016) E1424–E1433.

[39] C. Engelbrekt, K.H. Sørensen, J. Zhang, A.C. Welinder, P.S. Jensen, J. Ulstrup, Green synthesis of gold nanoparticles with starch-glucose and application in bioelectrochemistry, J. Mater. Chem. 19 (2009) 7839–7847.
[40] X. Xiao, H. Li, M. Wang, K. Zhang, P. Si, Examining the effects of self-assembled monolayers on nanoporous gold based amperometric glucose biosensors, Analyst 139 (2014) 488–494.
[41] N. Mano, A. De Poulpiquet, O_2 reduction in enzymatic biofuel cells, Chem. Rev. 118 (2018) 2392–2468.
[42] X. Xiao, D. Leech, J. Zhang, An oxygen-reducing biocathode with "oxygen tanks", Chem. Commun. 56 (2020) 9767–9770.
[43] I. Mazurenko, K. Monsalve, J. Rouhana, P. Parent, C. Laffon, A.Le Goff, S. Szunerits, R. Boukherroub, M.-T. Giudici-Orticoni, N. Mano, E. Lojou, How the Intricate interactions between carbon nanotubes and two bilirubin oxidases control direct and mediated O_2 reduction, ACS Appl. Mater. Interfaces 8 (2016) 23074–23085.
[44] K. KANO, T. IKEDA, Fundamentals and practices of mediated bioelectrocatalysis, Anal. Sci. 16 (2000) 1013–1021.
[45] X. Xiao, E. Magner, A biofuel cell in non-aqueous solution, Chem. Commun. 51 (2015) 13478–13480.
[46] A. Ciaccafava, P. Infossi, M. Ilbert, M. Guiral, S. Lecomte, M.T. Giudici-Orticoni, E. Lojou, Electrochemistry, AFM, PM-IRRA spectroscopy of immobilized hydrogenase: role of a hydrophobic helix in enzyme orientation for efficient H_2 oxidation, Angew. Chem. Int. Ed. 51 (2012) 953–956.
[47] F. Oteri, A. Ciaccafava, A. de Poulpiquet, M. Baaden, E. Lojou, S. Sacquin-Mora, The weak, fluctuating, dipole moment of membrane-bound hydrogenase from aquifex aeolicus accounts for its adaptability to charged electrodes, Phys. Chem. Chem. Phys. 16 (2014) 11318–11322.
[48] Y. Sugimoto, Y. Kitazumi, O. Shirai, M. Yamamoto, K. Kano, Role of 2-mercaptoethanol in direct electron transfer-type bioelectrocatalysis of fructose dehydrogenase at Au electrodes, Electrochim. Acta. 170 (2015) 242–247.
[49] I. Mazurenko, K. Monsalve, P. Infossi, M.T. Giudici-Orticoni, F. Topin, N. Mano, E. Lojou, Impact of substrate diffusion and enzyme distribution in 3D-porous electrodes: a combined electrochemical and modeling study of a thermostable H_2/O_2 enzymatic fuel cell, Energy Environ. Sci. 10 (2017) 1966–1982.
[50] J. Zhang, H.E.M. Christensen, B.L. Ooi, J. Ulstrup, *In situ* STM imaging and direct electrochemistry of pyrococcus furiosus ferredoxin assembled on thiolate–modified Au(111) surfaces, Langmuir 20 (2004) 10200–10207.
[51] A.C. Welinder, J. Zhang, A.G. Hansen, K. Moth-Poulsen, H.E.M. Christensen, A.M. Kuznetsov, T. Bjørnholm, J. Ulstrup, Voltammetry and electrocatalysis of achromobacter xylosoxidans copper nitrite reductase on functionalized Au(111)-electrode surfaces, Zeitschrift Für Phys. Chem. 221 (2007) 1343–1378.
[52] H. Xia, Y. Kitazumi, O. Shirai, K. Kano, Enhanced direct electron transfer-type bioelectrocatalysis of bilirubin oxidase on negatively charged aromatic compound-modified carbon electrode, J. Electroanal. Chem. 763 (2016) 104–109.
[53] N. Zhu, X. Hao, J. Ulstrup, Q. Chi, Single-nanoparticle resolved biomimetic long-range electron transfer and electrocatalysis of mixed-valence nanoparticles, ACS Catal. 6 (2016) 2728–2738.
[54] N. Zhu, J. Ulstrup, Q. Chi, Long-range interfacial electron transfer and electrocatalysis of molecular scale prussian blue nanoparticles linked to Au(111)-electrode surfaces by different chemical contacting groups, Russ. J. Electrochem. 53 (2017) 1204–1221.
[55] V. Climent, J. Zhang, E.P. Friis, L.H. Østergaard, J. Ulstrup, Voltammetry and single-molecule *in situ* scanning tunneling microscopy of laccases and bilirubin oxidase in electrocatalytic dioxygen reduction on au(111) single-crystal electrodes, J. Phys. Chem. C 116 (2012) 1232–1243.
[56] Q. Chi, J. Zhang, J.E.T. Andersen, J. Ulstrup, Ordered assembly and controlled electron transfer of the blue copper protein Azurin at gold (111) single-crystal substrates, J. Phys. Chem. B 105 (2001) 4669–4679.
[57] Y.I. Kharkats, H. Nielsen, J. Ulstrup, The effect of a low dielectric constant interlayer on the current—voltage relationship for simple electrode processes, J. Electroanal. Chem. Interfacial Electrochem. 169 (1984) 47–57.
[58] Q. Chi, J. Zhang, T. Arslan, L. Borg, G.W. Pedersen, H.E.M. Christensen, R.R. Nazmudtinov, J. Ulstrup, Approach to interfacial and intramolecular electron transfer of the diheme protein cytochrome *c4* assembled on Au(111) surfaces, J. Phys. Chem. B 114 (2010) 5617–5624.
[59] H.-G. Hong, W. Park, Electrochemical characteristics of hydroquinone-terminated self-assembled monolayers on gold, Langmuir 17 (2001) 2485–2492.
[60] X. Xiao, T. Siepenkoetter, R. Whelan, U. Salaj-Kosla, E. Magner, A continuous fluidic bioreactor utilising electrodeposited silica for lipase immobilisation onto nanoporous gold, J. Electroanal. Chem. 812 (2018) 180–185.
[61] K. Singh, T. McArdle, P.R. Sullivan, C.F. Blanford, Sources of activity loss in the fuel cell enzyme bilirubin oxidase, Energy Environ. Sci. 6 (2013) 2460–2464.
[62] C. Gutierrez-Sanchez, A. Ciaccafava, P.Y. Blanchard, K. Monsalve, M.T. Giudici-Orticoni, S. Lecomte, E. Lojou, Efficiency of enzymatic O_2 reduction by myrothecium verrucaria bilirubin oxidase probed by surface Plasmon resonance, PMIRRAS, and electrochemistry, ACS Catal. 6 (2016) 5482–5492.
[63] S.A. Shermukhamedov, R.R. Nazmutdinov, T.T. Zinkicheva, M.D. Bronshtein, J. Zhang, B. Mao, Z. Tian, J. Yan, D.Y. Wu, J. Ulstrup, Electronic spillover from a metallic nanoparticle: can simple electrochemical electron transfer processes be catalyzed by electronic coupling of a molecular scale gold nanoparticle simultaneously to the redox molecule and the electrode? J. Am. Chem. Soc. 142 (2020) 10646–10658.